# Liquid pattern and velocity field on a surface during spray impingement

Florian Schulz[1]*, Fabio J. W. A. Martins[1,2], Frank Beyrau[1]
1: Institute of Fluid Dynamics and Thermodynamics, Otto von Guericke University Magdeburg, Germany
2: Current address: Institute for Combustion and Gas Dynamics, University of Duisburg-Essen, Germany
* Correspondent author: florian.schulz@ovgu.de

**Keywords**: PIV, spray-wall interaction, wall film formation, light sheet illumination

ABSTRACT

The process of fuel injection and the associated wall impact is critical for the quality of combustion in engines. Secondary droplets and wall deposits are strongly related to incomplete combustion and soot emissions. To reduce harmful emissions and optimise the combustion, further investigations of the processes of spray impingement, secondary droplet formation and wall film formation are of central importance. In order to obtain a more comprehensive picture of the interaction between spray and wall, light sheet visualizations and particle image velocimetry (PIV) measurements were performed on an impinging gasoline spray within a conditioned pressure vessel. For this purpose, measurements were conducted both perpendicular to the jet axis and parallel to the wall. The focus here is on the conditions in a modern, homogeneously operated gasoline engine with a high-pressure injection valve with a well-known spray. The spray under investigation has already been studied using high-speed shadowgraphs and phase doppler anemometry measurements. The combination of the data allows validation and a better understanding of the present measurements. The injection pressure was 150 bar, the vessel temperature 80°C, and the nozzle-to-wall distance 35 mm. The vessel pressure was varied from 0.4 bar to 6 bar, which represents typical charge conditions in an engine. The measured data allowed the analysis of the internal structure of the spray and the quantification of the flow movements before and after the spray impact. The results obtained provided detailed new insights into the relevant sub-processes.

## 1. Introduction

In internal combustion engines, mixture formation is of decisive importance for the quality of combustion and the generation of exhaust emissions. Due to the limited size of the combustion chamber, the fuel spray reaches the chamber walls under various boundary conditions. The spray-wall interaction that occurs in this process is complex. This interaction leads to a deflection of the spray droplet spread and the generation of secondary droplets, which causes the formation of a wall film. As a result, the mixture quality is reduced locally and incomplete combustion with increased soot formation occurs in the resulting fuel-rich regions.

The optimisation of the spray-wall interaction process, with a reduction in the formation of large secondary droplets and a reduction in the mass of the wall film, would contribute significantly to cleaner combustion. Since internal combustion engines are the most widespread source of propulsion worldwide, there is great potential here - perhaps the greatest potential at present - for improving air quality in metropolitan areas. Due to the great importance of spray-wall interaction in petrol engines, there is a large amount of current research work in the field. The majority of the researchers use optical methods such as high-speed visualisation, laser-induced fluorescence (LIF), or refractive index matching method (RIM) to detect individual sub-processes during spray impact.

There are many studies on spray-wall interaction and wall film formation. The authors usually concentrate on individual influencing parameters and individual sub-processes. For example, Lamiel et al. (2021) investigated the influence of fuel pressure, fuel temperature, and nozzle-wall distance on the spread of an n-decane wall film using the RIM method. The fuel temperature is a very frequently investigated parameter since an increased fuel temperature can lead to the phenomenon of flash boiling. Among others, the publications of He et al. (2020), Li et al. (2020), and Schulz & Beyrau (2017) should be mentioned here, which look at both the spray and the resulting wall films. Beyond, measurements on the effect of the ambient pressure and the ambient temperature, and the spray characteristic were performed (Schulz & Beyrau, 2018a, 2018b; Schulz, Samenfink, Schmidt, & Beyrau, 2016). A less intensively studied parameter is wall roughness. According to Luo et al. (2017) this has a significant influence on spray dispersion and wall deposition. The influence of a pre-existing oil film on the wall surface is investigated by Wang et al. (2021).

The injection timing, and with it the nozzle-wall distance, is an important control variable in the engine. The effects on the wall film are investigated in Ding et al. (2020), Schulz & Beyrau (2018b, 2019). Pei et al. (2017) uses different fuels and finds correlations with secondary droplet formation using phase doppler anemometer (PDA) measurements. Luo et al. (2018) also analysed the droplet

sizes of primary and secondary droplets but using particle image analysis (PIA). The droplets can additionally interact via a crossflow effect, which was investigated by Si, Ashida et al. (2018), and Zhang et al. (2022). Since the deposition and evaporation of fluids are strongly determined by the prevailing boiling regime, an important focus is on the variation of the wall temperature and the determination of the heat transfer. Current findings in this regard can be found in the work of Mendieta et al. (2018), Schulz et al. (2014), Xia, Gao, & Li (2020), and Zhou et al. (2018). Based on the experiments, different approaches of simulation models have been developed (Biagiotti et al., 2021; Jüngst et al., 2021; Lamiel et al., 2017). However, due to the complexity of the processes, precise predictions are still difficult. The aforementioned investigations focus on the quantification of wall films and on photographs or shadowgraphs of a spray during wall impact from side views. These images are lign-of-sight integrated allowing only the outer boundaries of the spray to be captured. Few of the published spray images are of a quality that allows the internal structure of the spray to be identified and quantified. At the same time, there is a lack of measurements that look at the film movement during the spray-wall interaction, quantifying the spray motion parallel to the wall.

The present work aims to provide deeper insights of the structure within the spray through new perspectives, such as the horizontal section plane lying close above the wall surface. We performed light sheet visualizations and particle image velocimetry (PIV) measurements on an impinging gasoline spray within a conditioned pressure vessel using vertical and horizontal laser light sheets.

## 2 Setup and Method

The spray-wall interaction and the wall film formation depend on several parameters. In order to replicate the conditions in a homogeneously operated gasoline engine, but under well-defined boundary conditions, the PIV measurements were carried out in the pressure vessel shown in **Fig. 1** (left side). To limit the number of variables, the geometric boundary conditions in this investigation were matched to a research engine from Robert Bosch Company. This has an average-sized cylinder of 450 $cm^3$ with a centrally located injector. A detailed description of the research engine can be found in another publication (Köpple et al., 2013). A load condition in the high partial load range was selected as a representative engine operating point. This results in a fuel mass to be injected of 21.7 mg. Consequently, all the present experiments were carried out with this fuel mass. It should be noted that a symmetric six-hole injector was used in the experiments. Accordingly, 3.6 mg of fuel emerges from a single nozzle hole per injection.

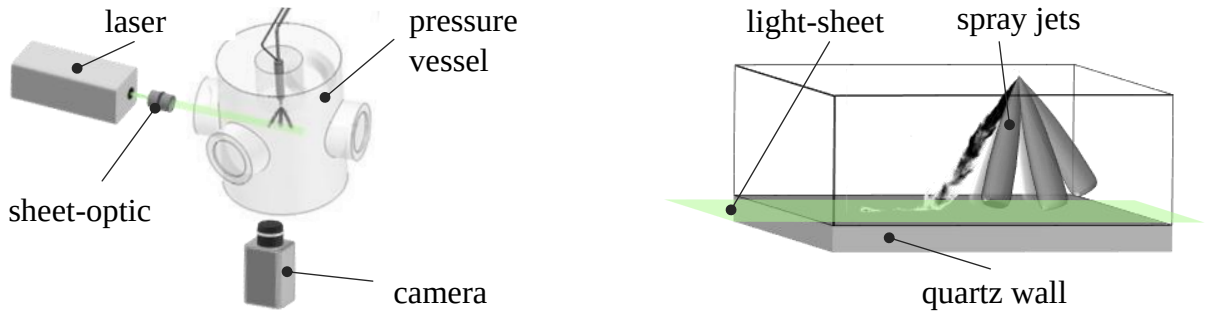


**Fig. 1** Pressure vessel with multiple optical accesses and setup for horizontal measurements (left); spray cone and light sheet above the impingement surface (right).

The present work focuses on the investigation of wall film formation in homogeneously operated engines in which the fuel is injected during the intake stroke. Thus, the cylinder pressure, depending on speed and load, is usually below the atmospheric pressure during injection. In this case pressures lower than 0.5 bar absolute pressure can be achieved. If, on the other hand, a turbocharger is used, the pressure in the cylinder at the time of injection can be more than 2 bar. For this reason, the vessel pressures for PIV measurements were set to the values of 0.4, 0.6, 1, 3, and 6 bar. The vessel pressure of 6 bar is intended to enable an estimate of the pressure influence in the case of increased turbocharging or for jet-guided combustion processes.

**Tab. 1** Boundary conditions of the setup and properties of the nozzle.

| **Property** | **Value** |
|---|---|
| vessel pressure (bar) | 0.4 / 0.6 / 1 / 3 / 6 |
| vessel temperature (°C) | 80 |
| Injector | Bosch HDEV5 |
| Number of holes | 6 |
| Geometric diameter (mm) | 0.21 |
| Average length (mm) | 0.21 |
| Hole shape | straight |
| Injected fuel mass (mg) | 21.7 |
| Rail pressure (bar) | 150 |
| Injection duration (ms) | 1.5 |
| Fuel | iso-octane |
| Nozzle-wall distance (mm) | 35 |

A significant part of the soot emissions measured in the standard cycles occurs during the warm-up phase of an engine when the in-engine temperatures are low. Derived from this, the vessel

temperature selected for the experimental investigations was 80°C. All essential operating parameters are summarised in **Tab. 1**.

In previous studies using the referred research engine, it was found that the soot emission decreases up to an injection timing of 300° CA BTDC (Kufferath et al., 2011). For later injection timing, the particle number concentration increases again due to the homogenisation time being too short for mixture formation. Furthermore, the soot emission in early injection timings essentially results from piston wetting. In order to simulate the influence of the injection timing in the wall film experiments, the distance between nozzle and wall can be varied. For the present investigation, we chose a nozzle-wall distance of 35 mm. This corresponds to an early to mean injection timing of about 315°CA BTDC.

To illustrate the spray produced, shadowgraph images for different ambient pressures are shown in **Fig. 2**. Since the images of individual spray jets show small variations in direction and density for each condition, ensemble-averaged images from 33 recordings are presented here. In the images, only 3 instead of 6 spray cones are visible, since the imaged beans of the symmetrical spray overlap. The images show the spray at the same time of 0.5 ms after the electrical activation of the solenoid valve, where "$t_{asoi}$" stands for "time after start of injection".

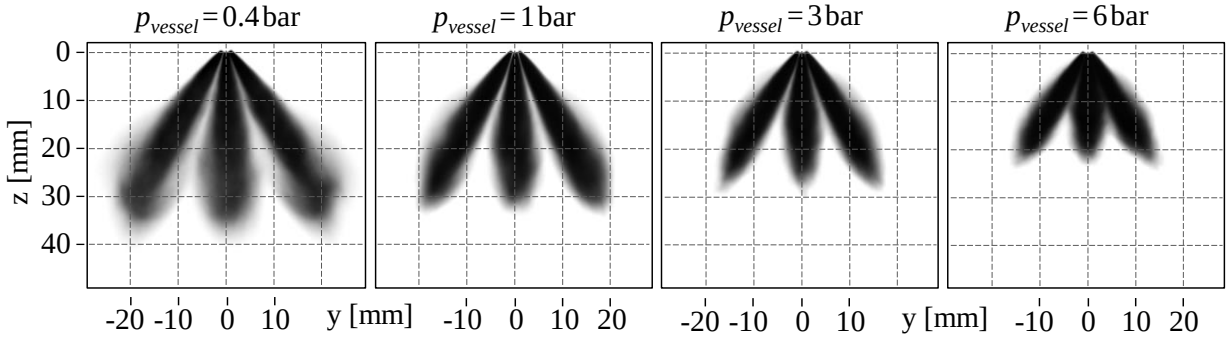


**Fig. 2** Ensemble-averaged shadow images of the spray for different vessel pressures at $t_{asoi}$ = 0.5 ms, $\vartheta_{vessel}$ = 80°C, $p_{rail}$ =150 bar.

In the present work, light sheet imaging and PIV are used to determine the spray structure and the droplet-cloud velocities during the spray-wall interaction. The PIV was used to measure the local spray velocities using a vertical light sheet and the flow velocity above the wall using the horizontal light sheet. For these measurements, the droplets within the spray served as particles in the PIV evaluation. It is anticipated that, since the droplets in the spray show a broad size distribution, the spray velocities are biased towards the biggest droplets due to the window cross-correlation procedure. Due to the temporally and spatially defined laser light sheet, the

experimental setup allows measurements of the inner structure of the spray, which presents density differences and the formation of droplet clusters.

The light source used was a Nd:YAG PIV double-pulse laser from Litron Laser Ltd. with a wavelength of 532nm, which can provide pulse energy of 135mJ at a maximum frequency of 15Hz. A light-sheet optic (f-50) was used to convert the laser beam into a sheet with a thickness of about 0.5mm in the investigation area. Two different light sheet arrangements were used: a vertical and a horizontal. In the vertical arrangement, the light sheet was positioned in such a way that it intersects the center of the spray jet, while, in the horizontal arrangement, the light sheet was guided parallel to the solid surface with its center at approximately 0.5mm from the wall. The laser and the camera were controlled via a programmable control unit (PTU) in combination with the control and evaluation software DaVis 8 from LaVision GmbH.

An Imager proX2M double-frame camera from LaVision GmbH with a resolution of 1600x1200 pixels in combination with a Panar T*85mm lens from Zeiss AG was used to capture the scattered light emitted by the spray drops. The camera was positioned below the pressure vessel for the horizontal light sheet measurements and on the side for the vertical light sheet ones. When positioning the camera on the side, it is important to note that the individual spray cones partially cover each other due to their arrangement in space, depending on the viewing direction. To be able to capture a larger part of the spray cone, a side camera was positioned at the vessel window at an angle of 70° to the measuring plane (see **Fig. 3**). To keep the entire image in focus under this non-perpendicular viewing angle, a Scheimpflug adapter was used. A calibration plate was employed to correct the image distortion due to the perspective and to assign the image scale for the velocity evaluation. Since the maximum frequency of the laser is limited to 15Hz, only one image can be recorded per injection. Different spray times were investigated by applying a time delay for the recording trigger relative to the start of injection.

Typical vertical light sheet images under the same operating condition are shown in **Fig. 3** to illustrate the variability of the spray. The four spray images have considerable differences in their appearance, although they were taken under the same constant boundary conditions and at the same time delay. The change of distribution is an important characteristic of the sprays of modern high-pressure injection valves. It is caused by a slight pendulum movement of the jets at the nozzle exit. These stochastic changes in the spray appearance make it difficult to compare the sprays under different operating conditions. Nevertheless, the four shown spray jets share the main macroscopic properties, such as the position of the spray impact at $x \approx 22$mm and the maximum penetration of the spray tip above the wall, which is located at $x \approx 35$mm.

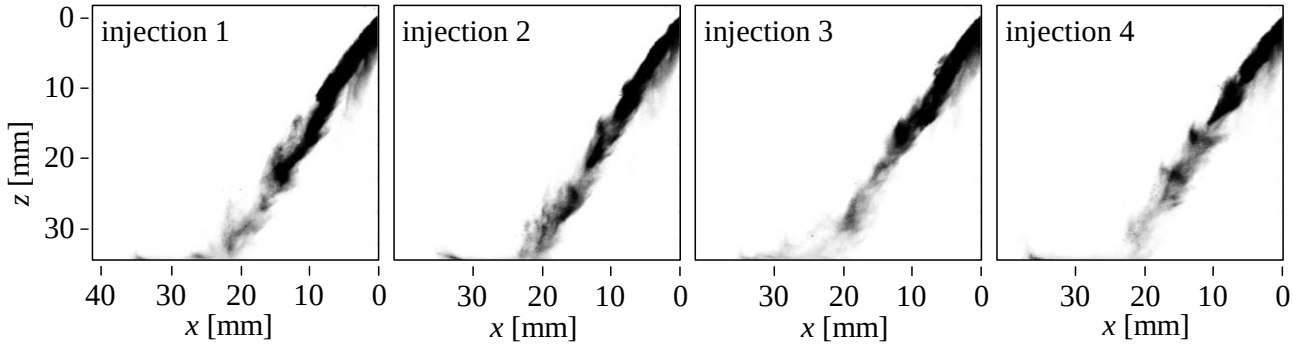


**Fig. 3** Vertical light sheet images of the spray-wall interaction of different injections under the same constant operating conditions at $t_{asoi}$ = 0.8 ms, $\vartheta_{vessel}$ = 80°C, $p_{rail}$ =150 bar.

The PIV algorithm is based on the position change of the particles or the position change of very small structures. It is important to point out that there are distinguishable microstructures in both the thin spray regions (light) and the dense spray regions (black). However, these are not discernible here in a linearly scaled grey level representation due to the prevailing large intensity differences. In the following, the false colour representation (see **Fig. 4**) is used instead of the grey level representation. This improves the visibility of structures in the very dense spray area at the nozzle outlet and very thin spray areas at a large distance from the nozzle.

A particular challenge in determining the velocity fields of sprays is the large velocity gradient. For example, under the conditions in **Fig. 3**, velocities of more than 120 m/s occur at the nozzle outlet and velocities of less than 40 m/s in the wall area. In order to reduce the velocity uncertainty near the wall, the time interval in the present investigation was optimised for these spray areas. To limit the velocity evaluation to the spray areas with particles, masks were applied. Since the macroscopic shape (width and orientation) of the spray changes under different boundary conditions, specially adapted masks were used in each case.

## 2 Results

The time sequence of a spray-wall interaction visualized using the light sheet technique is shown in **Fig. 4** for a rail pressure of 150 bar and a vessel pressure of 1 bar. It should be noted that each of the images originates from a separate injection. The individual images were selected to represent the majority of the repeat tests at the respective operating points. This approach is appropriate because, even under constant boundary conditions, fluctuations in the spray structure occur and averaging the exposures does not lead to meaningful images. The intensity of the detected Mie scattering, which correlates with the spray density, is illustrated with the aid of a false colour scale. When interpreting the colours, it should be noted that the intensities are not distributed linearly

on the colour scale. Shades of blue and black symbolize that more than 30% of the maximum camera intensity (16,384 count) has been reached, and cyan and yellow represent 13% and 1.5% of the maximum camera intensity, respectively.

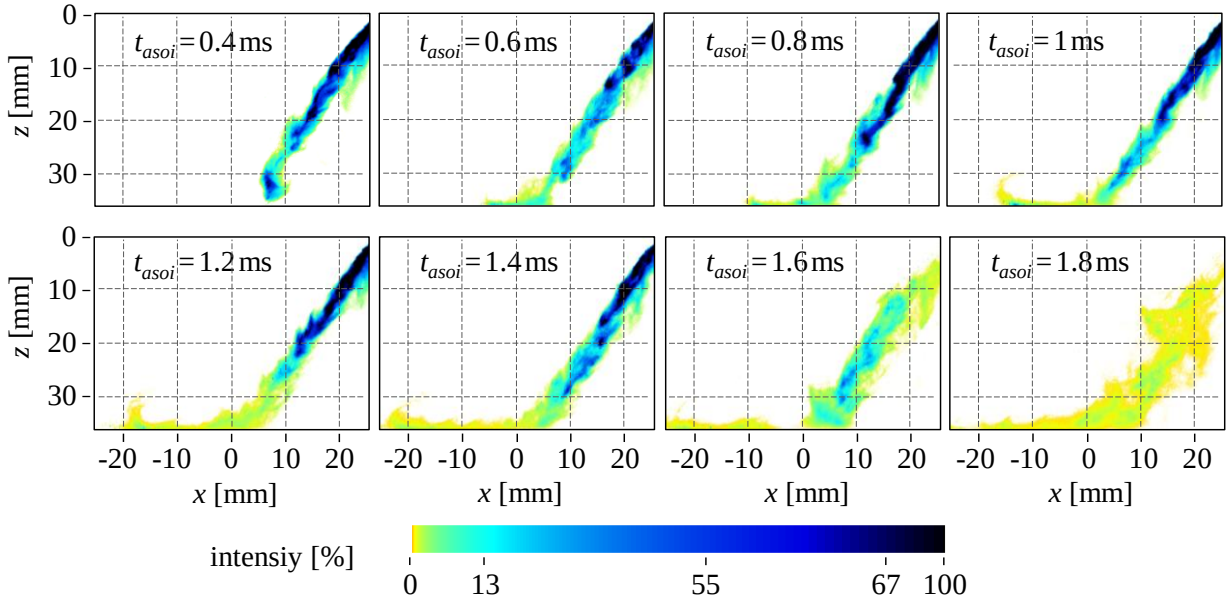


**Fig. 4** Light sheet images of the spray-wall interaction at different time steps.

During the injection process in **Fig. 4**, the spray density decreases at the position before impact. The reason for the accumulation of fuel in the spray front is the deceleration of the front spray droplets due to air resistance. The following droplets move in the slipstream of the leading droplets and approach the front. Over time, the cloud accumulated at the spray front continues to move and the following drops can move more freely, with decreased flow resistance. The characteristic that the first drops arriving at the wall have a lower velocity has a significant influence on the wall film formation. Using the averaged velocity of the total spray would lead to a misestimation of wall film formation. During the movement of the spray droplets along the wall surface, a clear lifting of the spray front from the wall and the formation of vortices only occurs in the late process starting at $t_{asoi}$=1 ms (time after start of injection). The size and height of the droplet cloud that slides above the wall increase with time, while the spray density above the wall decreases with time. This is partially expected because of the accumulated fuel in the spray front. A comparison of sample images for different vessel pressures is shown in **Fig. 5**. Due to the wide range of vessel pressures, the first wall contact of the spray occurs at different times. In order to represent the spray-wall interaction for each operating point, a suitable time after the start of

injection was selected in each case. The recording times shown tend to shift backward with increasing vessel pressure.

When looking at the spray pattern in the images in **Fig. 5**, it can be seen that the spray density increases with increasing vessel pressure from 0.4 to 1bar. A further increase in vessel pressure should also result in an increase in spray density, especially since the recording times are shifted backward and thus more fuel has already been injected at the time of recording. However, no significant increase in spray density is observed with a vessel pressure increase from 1 to 6bar. An important reason for these observations lies in the spray volumes, which are reflected in the respective spray angle and spray jet width. In fact, the spray jet angles as well as the spray jet width decrease from 0.4 to 1bar vessel pressure and subsequently increase again with further increasing vessel pressure. Assuming that the injected fuel is more or less uniformly distributed in the spray volume, the observed spray densities are plausible.

Particular attention should be paid to the spray at a vessel pressure of 0.4bar because there the spray structure deviates significantly from the spray structure occurring at higher vessel pressures. This indicates that a physical effect is gaining importance here, which plays only a minor role at vessel pressures above 1bar. One reason for the changed spray shape at 0.4bar is that with lowered ambient pressure, the force (the gradient in static pressure) that holds the spray together radially, also decreases.

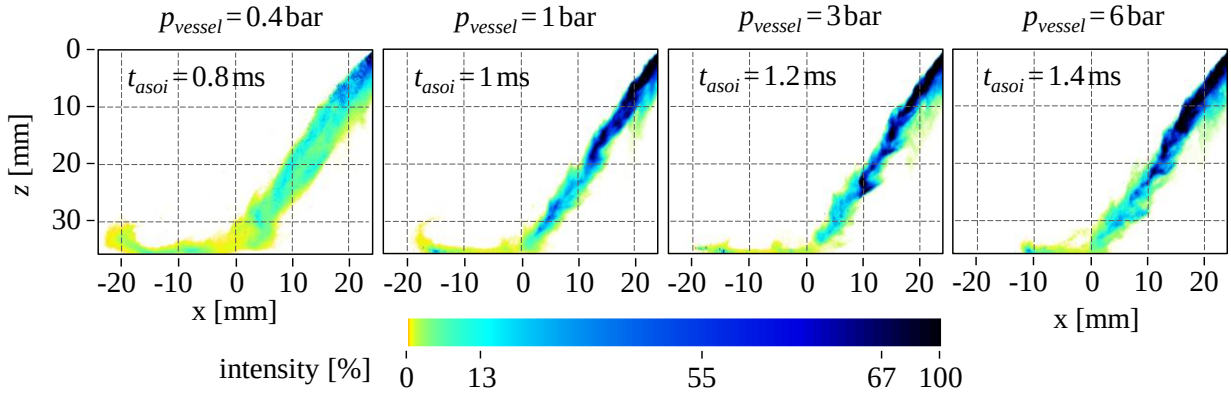


**Fig. 5** Light sheet images of the spray-wall interaction of a single spray jet for different vessel pressures.

Another significant aspect is the appearance of droplet clusters. In shadow images, especially in averaged images, the spray usually appears very homogeneous; this is not the case in the light sheet images. Clearly denser spray areas can be distinguished from less dense ones. The measured intensity differences are considerable, because, as previously discussed, the blue areas have four times the intensity of the cyan areas, and the cyan areas have approximately 10 times the intensity

of the yellow areas. One reason for the uneven spray distribution is the occurrence of a slight pendulum motion of the spray jets. This process is advantageous for mixture formation since it produces a larger spray volume, which in turn increases the ratio of air to fuel in the spray volume. The droplet clusters also affect the spray-wall interaction. In general, it is assumed that the spray density (or the droplet number density) as well as the droplet diameters and velocities have a significant influence on the secondary droplet formation and the heat transfer coefficient. Now, the droplet number density in the droplet clusters is significantly increased compared to other spray regions. At the same time, it can be assumed that, due to slipstream effects and coalescence, the droplet sizes and velocities in the droplet clusters also differ from those of other spray regions. Thus, the interaction of a droplet cluster with the wall takes place under very different conditions compared to the rest of the spray, which in turn can lead to higher heat transfer coefficients, for example.

The velocity fields corresponding to the fields in **Fig. 5** are shown in **Fig. 6**. It is important to recall that the time delay and processing were optimized for the velocity evaluation near the wall, therefore the much higher velocities displayed at the nozzle outlet may be subject to greater inaccuracy. Overall the velocities decrease with increasing vessel pressure, following the expectations. It should be emphasized that the velocity variations occurring within the spray are very large. The reason for this is again the presence of the droplet clusters. There is a tendency for higher velocities to occur in the denser spray areas. The velocities determined in the sprays essentially agree with the values determined in our PDA measurement campaign (not presented here).

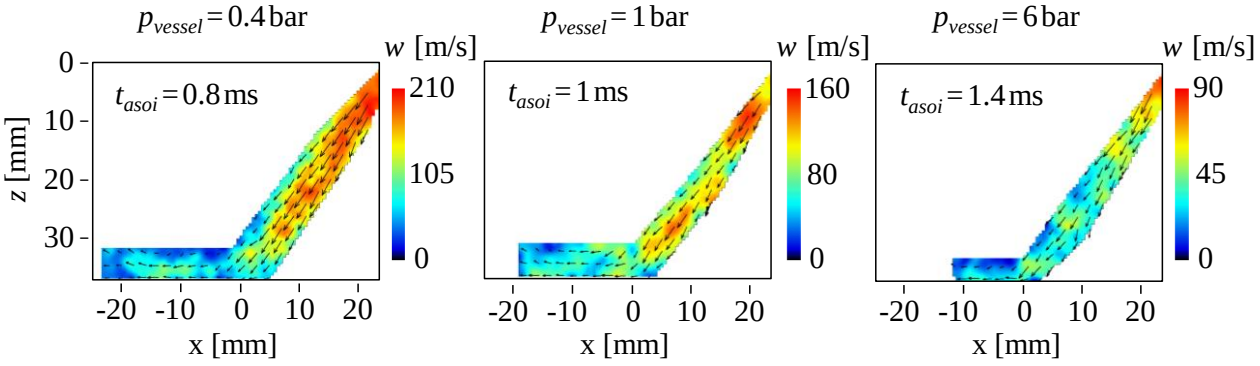


**Fig. 6** Comparison of velocity flow fields of an impinging spray jet for different vessel pressures.

In order to visualize the effect of the vessel pressure on the spray propagation on top of the wall surface, the images of three injections at a rail pressure of 150 bar, a nozzle-wall distance of 35 mm, and vessel pressures of 0.4, 1, and 6 bar are shown in **Fig. 7**. Here the spray droplets spread radially

around the jet impingement area and under the vessel pressures of 1 and 6 bar a ring-shaped cloud of droplets forms at the spray front. This is again caused by the increase in flow resistance due to the increase in vessel pressure, which in particular slows down the droplets at the spray front. This is also the cause of the strand formation that occurs with decreasing vessel pressure.

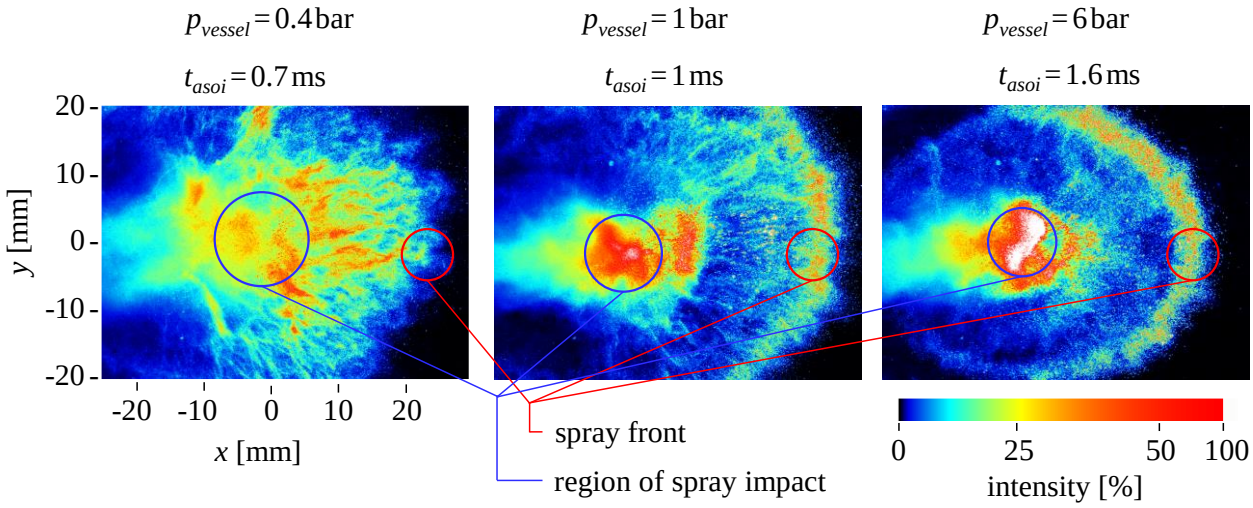


**Fig. 7** Horizontal light sheet images of an impacting spray on top of a quartz wall for different vessel pressures.

The velocity fields evaluated from the light sheet images in **Fig. 7** are shown in **Fig. 8**. The radial propagation of the spray drops on the wall surface mentioned above is confirmed by the velocity vectors. At the same time, it becomes clear that the flow velocity in the jet impact area, in which a wall film has already formed, is significantly lower than that of the radially spreading drops. This is plausible since the contact of the fuel with the wall immediately reduces the flow velocity due to the viscous effects.

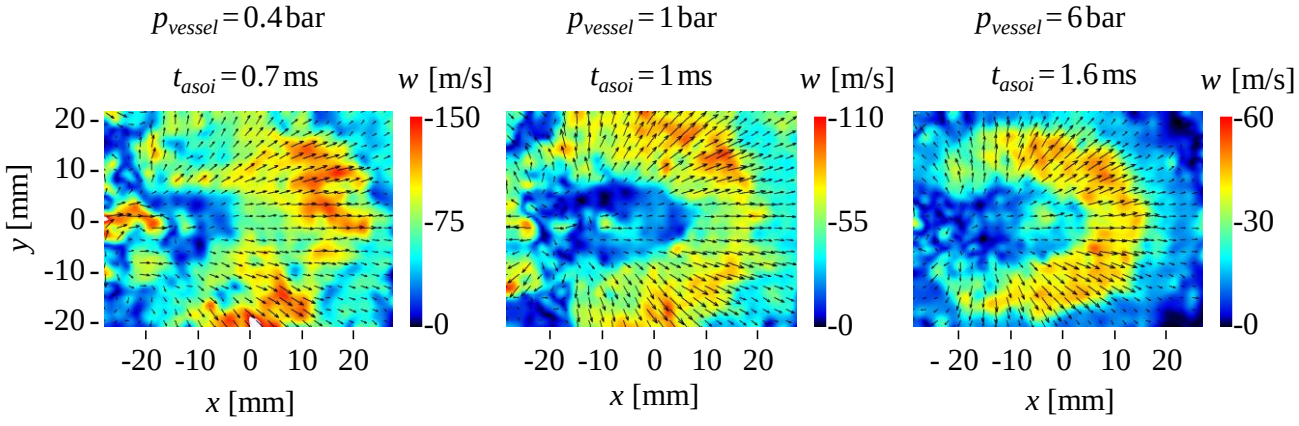


**Fig. 8** Comparison of velocity flow fields on top of the quartz wall for different vessel pressures.

The high flow velocities of the droplets spreading directly around the jet impingement area at vessel pressures of 1 and 6 bar are an indication that these are predominantly primary droplets. In comparison with the velocities in the jet before impingement (**Fig. 6**), these droplets have hardly lost any speed. At the same time, the spray density, which can be read from the scattered light intensity in **Fig. 7**, is very low in the areas with high flow velocity. As the droplets approach the propagation front of the spray, the velocity decreases significantly, and the spray density increases.

## 4. Conclusions

In the present study, light sheet images of a spray were acquired under different boundary conditions in a conditioned pressure vessel. Two measuring arrangements were used, firstly a vertical section through the spray axis, and secondly a horizontal section above the wall surface. From the images, the inner structures of the spray were analyzed and comparisons were made between the spray before and after impact. The results allowed for a better understanding of the formation of droplet clusters and the influence of the clusters on spray propagation and on spray-wall interaction.

In addition, PIV velocity fields were evaluated, estimating the movements of droplet groups during the spray-wall interaction. The velocities assigned to different spray areas provided a better understanding of the spray propagation and the spray-wall interaction. Of particular interest was the determination of the influence of various boundary conditions, such as ambient pressure, on the spray impingement process, since the investigated process is linked to the formation of soot particles in combustion engines.

## References

Biagiotti, F., Bonatesta, F., Tajdaran, S., Sciortino, D. D., Verma, S., Hopkins, E., . . . Haigh, R. (2021). Modelling liquid film in modern GDI engines and the impact on particulate matter emissions – Part 1. International Journal of Engine Research, 146808742110244. https://doi.org/10.1177/14680874211024476

Ding, C.-P., Vuilleumier, D., Kim, N., Reuss, D. L., Sjöberg, M., & Böhm, B. (2020). Effect of engine conditions and injection timing on piston-top fuel films for stratified direct-injection spark-ignition operation using E30. International Journal of Engine Research, 21(2), 302–318. https://doi.org/10.1177/1468087419869785

He, X., Li, Y., Liu, C., Sjöberg, M., Vuilleumier, D., Liu, F., & Yang, Q. (2020). Characteristics of spray and wall wetting under flash-boiling and non-flashing conditions at varying ambient pressures. Fuel, 264, 116683. https://doi.org/10.1016/j.fuel.2019.116683

Jüngst, N., Frapolli, N., Wright, Y. M., Boulouchos, K., & Kaiser, S. A. (2021). Experimental and numerical investigation of evaporating fuel films in combustion. Applications in Energy and Combustion Science, 7, 100033. https://doi.org/10.1016/j.jaecs.2021.100033

Köpple, F., Jochmann, P., Kufferath, A., & Bargende, M. (2013). Investigation of the Parameters Influencing the Spray-Wall Interaction in a GDI Engine - Prerequisite for the Prediction of Particulate Emissions by Numerical Simulation. SAE International Journal of Engines, 6(2), 911–925. https://doi.org/10.4271/2013-01-1089

Kufferath, A., Samenfink, W., Hammer, J., Schulz, F., Könnig, M., & Schmidt, J. (2011). Charakterisierung des Wandfilms relevanter Betriebsbedingungen für einen direkteinspritzenden Ottomotor als Grundlage zur Schadstoffminimierung. 10. Tagung Motorische Verbrennung.

Lamiel, Q., Lamarque, N., Hélie, J., & Legendre, D. (2017). Spreading model for wall films generated by high-pressure sprays. Ilass Europe. 28th european conference on Liquid Atomization and Spray Systems, 138–145. https://doi.org/10.4995/ILASS2017.2017.4999

Lamiel, Q., Lamarque, N., Hélie, J., & Legendre, D. (2021). On the spreading of high-pressure spray-generated liquid wall films. International Journal of Multiphase Flow, 139, 103619. https://doi.org/10.1016/j.ijmultiphaseflow.2021.103619

Li, X., Di Xiao, Parrish, S. E., Grover, R. O., Hung, D. L. S., & Xu, M. (2020). Dynamics of spray impingement wall film under cold start conditions. International Journal of Engine Research, 21(2), 319–329. https://doi.org/10.1177/1468087419859682

Luo, H., Nishida, K., Uchitomi, S., Ogata, Y., Zhang, W., & Fujikawa, T. (2018). Microscopic behavior of spray droplets under flat-wall impinging condition. Fuel, 219, 467–476. https://doi.org/10.1016/j.fuel.2018.01.059

Luo, H., Uchitomi, S., Nishida, K., Ogata, Y., Zhang, W., & Fujikawa, T. (2017). Experimental investigation on fuel film formation by spray impingement on flat walls with different surface roughness. Atomization and Sprays, 27(7), 611–628. https://doi.org/10.1615/AtomizSpr.2017019706

Mendieta, A., Dragomirov, P., Schulz, F., Beyrau, F., Samenfink, W., & Schuenemann, E. (2018). Laser-Based Measurements of Surface Cooling Following Fuel Spray Impingement. SAE Technical Paper. (2018-01-0273). Retrieved from https://trid.trb.org/view/1560698

Pei, Y., Qin, J., Li, X., Zhang, D., Wang, K., & Liu, Y. (2017). Experimental investigation on free and impingement spray fueled with methanol, ethanol, isooctane, TRF and gasoline. Fuel, 208, 174–183. https://doi.org/10.1016/j.fuel.2017.07.011

Schulz, F., & Beyrau, F. (2017). The influence of flash-boiling on spray-targeting and fuel film formation. Fuel, 208, 587–594. https://doi.org/10.1016/j.fuel.2017.07.047

Schulz, F., & Beyrau, F. (2018a). Comparison of the Spray and the Spray/Wall Interaction of Two Gasoline Injectors. International Journal of Automotive Technology, 19(4), 615–622. https://doi.org/10.1007/s12239-018-0058-4

Schulz, F., & Beyrau, F. (2018b, April 3). Systematic Investigation of Fuel Film Evaporation (SAE Technical Paper No. 2018-01-0310). Retrieved from https://www.sae.org/publications/technical-papers/content/2018-01-0310/ https://doi.org/10.4271/2018-01-0310

Schulz, F., & Beyrau, F. (2019). The effect of operating parameters on the formation of fuel wall films as a basis for the reduction of engine particulate emissions. Fuel, 238, 375–384. https://doi.org/10.1016/j.fuel.2018.10.109

Schulz, F., Samenfink, W., Schmidt, J., & Beyrau, F. (2016). Systematic LIF fuel wall film investigation. Fuel, 172, 284–292. https://doi.org/10.1016/j.fuel.2016.01.017

Schulz, F., Schmidt, J., Kufferath, A., & Samenfink, W. (2014). Gasoline Wall Films and Spray/Wall Interaction Analyzed by Infrared Thermography. SAE International Journal of Engines, 7(3), 1165–1177. https://doi.org/10.4271/2014-01-1446

Si, Z., Ashida, Y., Shimasaki, N., Nishida, K., & Ogata, Y. (2018). Effect of cross-flow on spray structure, droplet diameter and velocity of impinging spray. Fuel, 234, 592–603. https://doi.org/10.1016/j.fuel.2018.07.061

Wang, C., Pei, Y., Qin, J., Peng, Z., Liu, Y., Xu, K., & Ye, Z. (2021). Laser induced fluorescence investigation on deposited fuel film from spray impingement on viscous film over a solid wall. Energy, 231, 120893. https://doi.org/10.1016/j.energy.2021.120893

Xia, Y., Gao, X., & Li, R. (2020). Management of surface cooling non-uniformity in spray cooling. Applied Thermal Engineering, 180, 115819. https://doi.org/10.1016/j.applthermaleng.2020.115819

Zhang, G., Shi, P., Luo, H., Ogata, Y., & Nishida, K. (2022). Investigation on fuel adhesion characteristics of wall-impingement spray under cross-flow conditions. Fuel, 320, 123925. https://doi.org/10.1016/j.fuel.2022.123925

Zhou, Z.-F., Mohd Murad, S. H., Tian, J.-M., Camm, J., & Stone, R. (2018). Experimental investigation on heat transfer of n-pentane spray impingement on piston surface. Applied Thermal Engineering, 138, 197–206. https://doi.org/10.1016/j.applthermaleng.2018.04.059